Papillary muscles, ventricular loading, and atrial remodelling as beat-to-beat determinants of functional mitral regurgitation: an exploratory Granger causality study

Csilla A. Eötvös1, * MD; Teodora Avram1, MD; Eric Daniel Blendea2, Matei Ioan Munteanu3, Adrian Florin Bubuianu4, Madalina P. Moldovan1, MD; Petra Hedesiu5, Roxana D. Lazar1, MD; Iulia G. Zehan1, MD; Adriana D. Sarb1, MD; Giorgia Coseriu1, MD; Patricia Schiop-Tentea1, MD; Diana L. Mocan-Hognogi6, MD PhD; Roxana Chiorescu6, MD PhD; Sorin Pop6, MD; Laura Diosan, PhD4, E. Kevin Heist7, MD PhD; Dan Blendea,1, MD PhD.

1 Department of Internal Medicine and Doctoral School, “Iuliu Hatieganu”, University of Medicine and Pharmacy Cluj-Napoca, Romania

2 Emil Racovita National College, Cluj-Napoca, Romania

3. Institut Polytechnique, Paris, France

4 Department of Computer Science, Babes Bolyai University, Cluj-Napoca, Romania

5. School of Engineering, Columbia University, New York, USA

6 Emergency Clinical County Hospital, “Iuliu Hatieganu” University of Medicine and Pharmacy, Cluj-Napoca, Romania

7 Massachusetts General Hospital, Harvard Medical School, Boston, MA 02215, USA

This work was conducted at the Iuliu Hatieganu University of Medicine and Pharmacy and the Babes-Bolyai University in Cluj-Napoca, Romania, as well as at Massachusetts General Hospital, Harvard Medical School, Boston, MA, USA.

* Author to whom correspondence should be addressed.

Csilla A. Eötvös1, MD.

Iuliu Hatieganu University of Medicine and Pharmacy, str. Victor Babes 8, 400012 Cluj-Napoca, Romania

Email: csilla.andrea18@gmail.com; eotvos.csilla.andrea@elearn.umfcluj.ro

Word count: ~4500

Abbreviations

AFMR = atrial functional mitral regurgitation; ALPM = anterolateral papillary muscle; FMR = functional mitral regurgitation; LA = left atrium; LV = left ventricle; MR = mitral regurgitation; PM = papillary muscle; PMPM = posteromedial papillary muscle; VAR = vector autoregressive; VFMR = ventricular functional mitral regurgitation.

Abstract

Background

Functional mitral regurgitation results from interacting mechanisms whose relative contributions vary between atrial and ventricular subtypes and shift dynamically within each heartbeat, producing temporal patterns that static analyses cannot capture.

Objectives

To identify which structural determinants predict mitral regurgitation variability beat to beat using Granger causality within vector autoregression, focusing on papillary muscle dynamics across subtypes.

Methods

Frame-level echocardiographic time series from 41 patients (21 atrial, 20 ventricular; 1,959 frames) were z-score standardised within patient. Individual (lag 3) and pooled (lag 2) vector autoregression models tested whether left ventricular volume, left atrial volume, papillary muscle length, and annulus diameter Granger-predict mitral regurgitation area.

Results

Individual models revealed marked heterogeneity. In pooled analysis, left ventricular volume was the strongest Granger predictor at short lags (atrial p=0.011; ventricular p=0.006), while left atrial volume emerged at longer lags (lag 7: atrial p=0.043; ventricular p=0.011). Systolic papillary muscle length was not predictive. Full-cycle analysis revealed a subtype-specific dissociation: papillary muscle length Granger-predicted regurgitation only in the

ventricular subtype (p=0.001), while regurgitation predicted papillary muscle displacement only in the atrial subtype (p<0.001). Left ventricular volume dominated within-beat prediction but lost cross-beat relevance in the ventricular subtype, while left atrial volume gained cross-beat predictive relevance in the atrial subtype. No structural determinant correlated with severity cross-sectionally.

Conclusions

Beat-to-beat vector autoregression and Granger modelling reveals heterogeneous, subtype-specific temporal patterns with distinct temporal windows of predictability for ventricular loading and papillary geometry. This framework may support patient-specific temporal phenotyping of functional mitral regurgitation.

Keywords: Granger causality; papillary muscle; beat-to-beat variability; vector autoregression; atrial functional MR; ventricular functional MR

Graphical Abstract

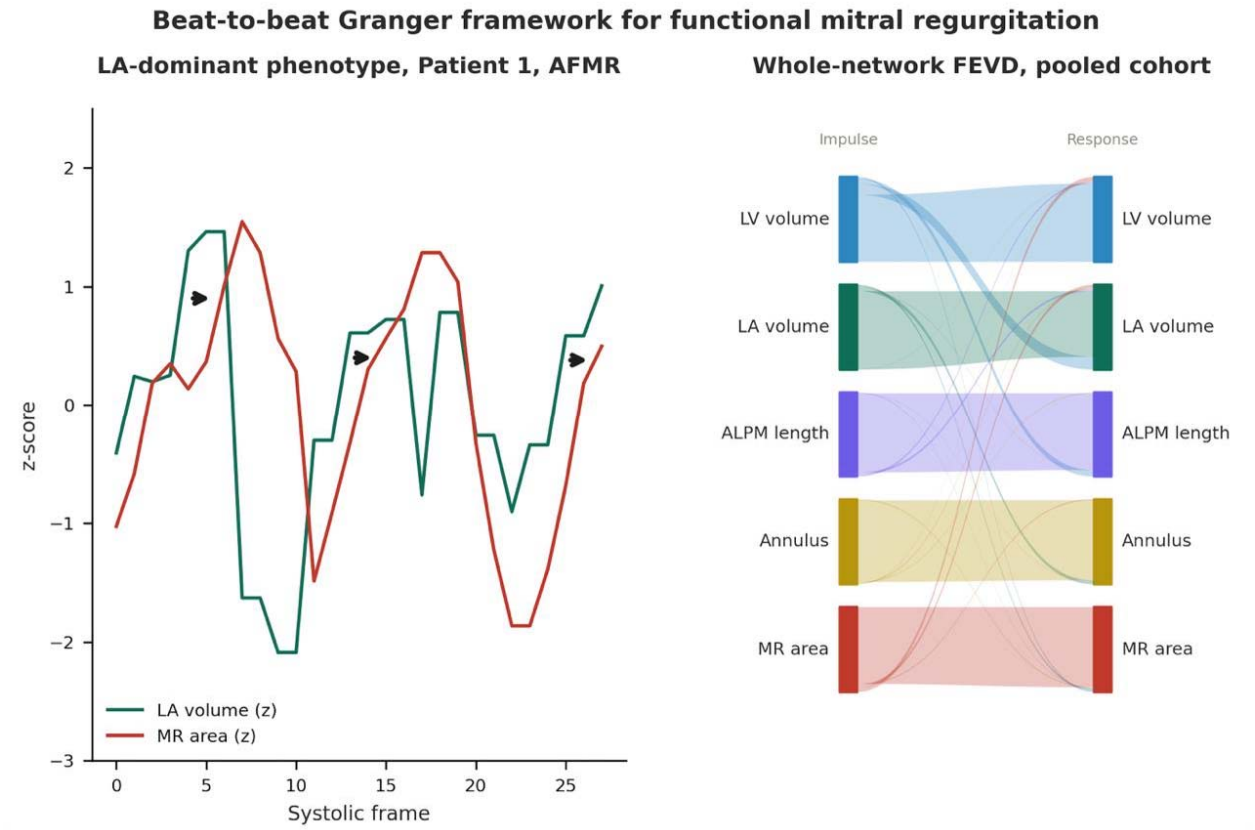

Introduction

Functional mitral regurgitation (FMR) affects up to 10% of heart failure patients and independently worsens outcomes.(1) Unlike primary mitral regurgitation (MR), the leaflets are intact; the regurgitation results from ventricular or atrial remodelling that distorts mitral apparatus geometry.(2) Two subtypes are recognised: ventricular FMR (VFMR), driven by left ventricular (LV) dilatation and apical papillary muscle (PM) displacement; and atrial FMR (AFMR), driven by left atrial (LA) enlargement(3) and annular dilatation in the context of atrial fibrillation or heart failure with preserved ejection fraction.(4, 5)

A subset of patients responds inadequately to treatment, reflecting mechanistic heterogeneity (Figure 1-Panel A).(6) Functional MR represents the common endpoint of multiple interacting pathways: ventricular volume overload, annular dilatation, leaflet tethering, and PM displacement, whose relative contributions vary substantially between patients.(5, 7) COAPT(8) and MITRA-FR(9) illustrate this heterogeneity: morphologically similar patients may have fundamentally different dominant drivers and respond differently to the same intervention. A therapy targeting annular geometry will fail if the primary driver is PM tethering. Identifying the dominant mechanism individually remains an unresolved challenge.

Papillary muscles are mechanistically central to FMR but clinically undercharacterised. In VFMR, PM displacement increases leaflet tethering, a well-established mechanism in post-infarction MR and dilated cardiomyopathy.(5, 7, 10) Two critical questions remain. First, it is unclear whether PM displacement actively modulates beat-to-beat MR variability or simply establishes a fixed tethering substrate determining mean severity; only in the former case would PM-targeted therapy reduce dynamic MR fluctuation. Second, whether PM contribute dynamically to MR in AFMR remains unknown.

Static cross-sectional measurements capture geometric correlates of MR severity but cannot establish directionality: the same correlation may reflect tethering causing MR, remodelling causing both, or MR-driven overload displacing the PMs. Disentangling these relationships requires a framework that accounts for temporal precedence and quantifies each determinant's independent contribution. Granger causality within vector autoregressive (VAR) modelling of beat-to-beat time series provides exactly this, given the substantial beat-to-beat variability of MR.(11-14) Developed in econometrics(15) and applied in cardiovascular physiology(16-18), Granger causality tests whether a variable's past improves prediction of another beyond its own history. Throughout, 'causality' denotes temporal predictability, not mechanistic causation (Figure 1 – Panel B).

We hypothesized that beat-to-beat MR variability reflects temporally structured interactions among ventricular loading, atrial remodelling, annular geometry, and PM dynamics, differing between AFMR and VFMR.

Methods

Study population and echocardiographic data acquisition

We retrospectively analysed transthoracic echocardiograms from 41 patients (21 AFMR, 20 VFMR; 8 in atrial fibrillation during examination) enrolled at three university hospitals in Cluj County, Romania (Figure 2). Ventricular FMR required LV dilatation or dysfunction with intact leaflets; AFMR required LA enlargement with preserved or mildly reduced LV function without significant ventricular remodelling. Baseline structural variables included PM length(19), tenting height(20), and annular diameter (Figure 3). Per patient, two or more consecutive cycles were analysed frame-by-frame at 30 fps (Figure 1 – Panel C), yielding 19–329 frames (1,959 total). 'Frame-level' denotes within-cycle resolution; 'cross-beat' inter-cycle dynamics (lag 6 ≈ 200 ms); 'beat-to-beat' both timescales. Measurements were performed by three observers (one per patient).

Variable selection

Four determinants were selected: LV volume, LA volume, annulus diameter, and ALPM length, measured from the LV apex to the mid-basal papillary muscle insertion in the four-chamber view (Figure 3), representing ventricular loading, atrial remodelling, annular geometry, and PM mechanics respectively.

Frame-by-frame longitudinal measurements

Five variables were measured every frame: MR jet area (cm^2), LV volume (ml), LA volume (ml), annulus diameter (cm), and ALPM length (mm) (19). Tenting height was measured in systolic frames only. Frames were classified as systolic or diastolic. Mitral regurgitant jet area served as a temporal variability surrogate, not an absolute severity metric; within-patient relative fluctuations remain informative despite load dependence. Diastolic MR area was zero when no regurgitant flow was present; non-zero values were retained. Pooled models used a continuous frame index with patient fixed effects.

Within-patient z-score standardisation

All time-series variables were z-score standardised within patient to remove between-subject magnitude differences while preserving temporal variability. Variables spanning the full cardiac cycle used all frames; MR area used systolic frames only, avoiding distortion from phase-restricted measurement.

Statistical analysis

Pooled VAR models tested Granger-predictive relationships among all determinants and MR area. All analyses are exploratory. Baseline characteristics are mean (SD) or count (percentage), compared by t-tests and chi-square tests.

Individual-patient vector autoregression

A VAR model was fitted per patient (minimum 20 systolic frames), expressing each variable as a function of its own and all other variables' lagged values. Endogenous variables: MR area, LV volume, LA volume, and ALPM length (three-variable model when ALPM not visible). With short series (median 29 frames), individual models primarily illustrate heterogeneity. A fixed lag of 3 (~100 ms at 30 fps) was used for all patients, maximising the temporal window for Granger causality detection within the constraint of short series (Table 2). Stability verified by eigenvalue analysis.

Granger causality was assessed using Wald chi-square tests ($p<0.05$ threshold). Sensitivity analyses with alternative lag orders yielded directionally consistent results. Forecast error variance decomposition (FEVD) at horizon 5 quantified how much of the variability in predicting future MR area is attributable to each predictor. Orthogonalised impulse response functions (OIRFs) characterised whether a sudden increase in each predictor is followed by a rise or fall in MR area.

Patients were classified by dominant Granger predictor: LV-dominant, PM-dominant, LA-dominant, LV+PM, LA+LV, LA+PM, or Neither. These labels represent descriptive clustering of predictive patterns, not stable mechanistic phenotypes. Unstable models (eigenvalue ≥1) are marked with † in Table 2 and interpreted with caution.

Pooled panel vector autoregression

A pooled panel VAR was estimated separately for AFMR, VFMR, and the combined cohort, using systolic frames from patients with ALPM visibility. Five endogenous variables were included: MR area, LV volume, LA volume, systolic ALPM length, and annulus diameter, with lag 2 (~67ms at 30 fps). Patient indicator variables served as fixed effects. Robustness was assessed at lag orders 2, 6 (~200 ms, approximately one cardiac cycle), and 7 (~233 ms, cross-beat). The global systolic frame counter served as the time variable.

Granger causality, FEVD, and OIRF were extracted as for individual models. All analyses were performed in Stata 19 (StataCorp, College Station, TX). A two-sided $p<0.05$ was considered significant throughout.

Results

Baseline Characteristics (Table 1)

Atrial FMR patients were older, predominantly female, with more atrial fibrillation; VFMR patients predominantly male with more coronary disease. Moderate–severe MR in VFMR was associated with wider QRS, more LBBB, larger LV dimensions, lower ejection fraction, and thinner septum (Table 1). No comparable differences appeared in AFMR.

No PM variable differed significantly by MR severity despite numerical trends. Among the four VAR determinants, none showed a consistent cross-sectional association with severity (Table 1), reinforcing the need for dynamic analysis.

Individual Patient VAR Analysis (Table 2)

Patients with sufficient systolic frames underwent individual VAR(3) analysis (~100 ms temporal window; Figure 4). Of 34 analysable patients, 25 had stable models at lag 3; those without ALPM visibility used a reduced three-variable model (Table 2).

The most common phenotype was "neither" in both groups, reflecting limited power with short series. These should be interpreted as illustrative rather than definitive. Among identifiable phenotypes, LV and LA involvement were equally represented in both subtypes. Papillary muscle involvement was more frequent in VFMR (6 of 10 patients with PM-containing phenotypes; 4 of 6 among stable models), suggesting that active beat-to-beat PM–MR coupling is primarily ventricular in this cohort (Table 2).

Patient 40 (VFMR), despite clear structural PM pathology (post-MI dysfunction, elevated tenting), showed no Granger predictors, illustrating that fixed geometric deformation does not necessarily produce active dynamic PM–MR coupling.

Measurement Reproducibility

Intraobserver reproducibility (7 patients, 70 paired observations) yielded excellent ICC for MR area (0.986), LA volume (0.981), LV volume (0.971), and good ICC for ALPM length (0.890), with negligible mean bias across all variables (detailed Bland–Altman results in Supplementary Table S1).

Pooled VAR Analysis

Pooled VAR analysed systolic frames from 37 patients with ALPM visibility. After lag initialisation, 456 AFMR, 702 VFMR, and 1,160 overall observations remained (Table 3). All models were stable.

LV volume was the strongest individual Granger predictor in both subtypes (AFMR p=0.011; VFMR p=0.006); systolic ALPM was not predictive (Table 3). The joint test of all four predictors was significant in VFMR (p=0.029) and overall (p<0.001) but not in AFMR (p=0.252), likely reflecting limited power in the smaller AFMR sample (456 observations, 17 patients) spread across eight degrees of freedom rather than absence of multifactorial coupling. This suggests PM displacement primarily establishes the structural tethering substrate rather than actively driving beat-to-beat MR variability, consistent with the rarity of purely PM-dominant phenotypes in individual analysis.

Lag-specific results

Table 3 presents results across three temporal windows: lag 2 (~67 ms, within-beat), lag 6 (~200 ms, approximately one cardiac cycle), and lag 7 (~233 ms, cross-beat).

Systolic ALPM was not a significant Granger predictor in any pooled model at any lag, with FEVD contributions below 1.5% (Table 3).

Reverse Granger testing revealed that MR area predicted ALPM displacement at longer lags in both subtypes (AFMR lag 5 p=0.010; VFMR lag 4 p=0.046, lag 5 p=0.023), indicating that the temporal relationship flows from regurgitation to papillary muscle repositioning rather than the reverse. Additionally, LV volume strongly Granger-predicted ALPM in AFMR (p<0.001 at lags 2-5) while annulus diameter predicted ALPM in VFMR (p=0.002-0.024), suggesting subtype-specific pathways to papillary muscle displacement.

Full-cycle papillary muscle analysis

Because the primary pooled model analysed systolic frames only, a supplementary full-cycle analysis tested whether diastolic papillary muscle dynamics contribute to MR prediction. Multivariate pooled VAR models (MR area, LA volume, LV volume, ALPM length; patient fixed effects) were fitted at lags 1–20 for each subtype (17 AFMR, 20 VFMR patients). ALPM Granger-predicted MR only in VFMR (lag 1 p=0.001; lags 1–4 and 7 significant; 0/20 lags significant in AFMR), with FEVD contributions of 1.3–1.5% (Table 3). The reverse direction showed a mirror-image: MR predicted ALPM at all 20 lags in AFMR (p<0.001 from lag 2) but at none in VFMR. ALPM variance was 66–72% self-driven in AFMR (LV volume 17–20%, LA volume 6–9%) versus 95–96% in VFMR (Table 3).

Lag-specific temporal windows

At lag 2, LV volume dominated MR prediction in both subtypes (AFMR p=0.011; VFMR p=0.006); ALPM showed no within-beat contribution. At lag 6, a subtype-specific pattern emerged: LA volume gained significance in both subtypes (AFMR p=0.033; VFMR p=0.004) while LV volume lost predictive value in VFMR (p=0.328) but persisted in AFMR (p=0.012). Annulus diameter became significant in VFMR at lags 6 and 7 (p=0.017 and p=0.011).

By lag 7, LA volume reached significance in AFMR (p=0.043), representing the first temporal window at which atrial remodelling independently predicted MR in this subtype. ALPM remained non-predictive across all lags in both subtypes (Table 3). These temporal patterns suggest that ventricular loading operates at rapid haemodynamic timescales, whereas atrial remodelling exerts delayed cross-beat effects.

Whole-network FEVD visualised the full causal architecture (Figure 5). MR area was overwhelmingly self-driven (AFMR 97.3%, VFMR 96.6%), with LV volume and LA volume as the largest external contributors. ALPM length explained less than 1% of MR variance in both subtypes.

Discussion

Beat-to-beat VAR/Granger analysis reveals that FMR determinants interact dynamically across multiple timescales. However, given the exploratory design and the conditional nature of Granger inference, these findings describe temporal predictive patterns rather than stable mechanistic phenotypes.

Individual phenotypic heterogeneity

Although most individual patients showed no dominant predictor, pooled analysis confirmed LV volume as a consistent driver. The individual-level heterogeneity likely reflects distributed multifactorial coupling rather than absent physiological influence.

LV and LA involvement were equally frequent among identifiable phenotypes in both subtypes, whereas papillary muscle involvement appeared predominantly in VFMR.

Papillary muscle displacement appears to establish the tethering substrate on which ventricular loading operates. Full-cycle analysis added nuance: ALPM predicted MR in VFMR at short lags, indicating that the diastole-to-systole transition carries predictive information that systolic-only analysis truncates. The variance contribution was modest — a small independent PM input superimposed on dominant ventricular loading. In AFMR, the relationship ran exclusively in reverse, with regurgitation driving PM dynamics. PM-targeted therapy may therefore modify this substrate, which contributes modestly but independently to beat-to-beat regurgitation in VFMR.

Systolic ALPM and lag-specific temporal patterns

Systolic ALPM was not predictive at any lag (2, 6, 7), confirming the tethering-substrate interpretation. Subtype-specific temporal windows emerged (Table 3): LV volume dominated within-beat prediction but lost cross-beat relevance in VFMR, while LA volume reached significance in AFMR only at lag 7.

In the full-cycle model, MR predicted ALPM displacement at all lags in AFMR but at none in VFMR (Table 3). In the systolic pooled model, reverse causality emerged in both subtypes at longer lags (AFMR lag 5 p=0.010; VFMR lag 4 p=0.046), suggesting that, within systole, the temporal relationship flows from regurgitation to papillary muscle repositioning. This unidirectional pattern in AFMR suggests PM displacement is a downstream consequence of volume overload rather than an upstream driver.

The pathways to papillary muscle displacement differed by subtype. In AFMR, LV volume was the dominant predictor of ALPM, consistent with volume-mediated remodelling driving PM displacement even in the atrial subtype. In VFMR, annulus diameter rather than LV volume predicted ALPM, suggesting that annular dilatation and subvalvular geometry are more tightly coupled in ventricular remodelling.

Variance decomposition (Figure 5) confirmed MR was predominantly self-driven. LV and LA volume were the primary external influences. ALPM explained under 1% of MR variance in either subtype, reinforcing the tethering-substrate interpretation.

Clinical implications and the COAPT/MITRA-FR paradox

This heterogeneity may partly explain divergent responses in COAPT(8) and MITRA-FR(9): patients with similar static geometry may differ in temporal coupling. When ventricular loading drives variability, remodelling-targeted therapies may be preferred; when tethering predominates, PM-targeted or mitral apparatus interventions may be more effective, given that PM displacement contributes modestly but independently in VFMR.(8, 9, 21, 22) Temporal phenotyping could provide stratification beyond static anatomy, pending prospective validation.

Beat-to-beat Granger causality as a reusable framework

The beat-to-beat VAR/Granger framework introduced here is not disease-specific: applied to frame-level echocardiographic data, it enables patient-specific temporal profiling of competing pathways. If validated, it could support mechanistic stratification and assessment of which pathways are attenuated by intervention.

Limitations

First, this study is exploratory and hypothesis-generating; Granger "causality" denotes temporal predictive content conditional on included variables, not mechanistic causation, and may reflect unmeasured confounding. No formal multiple comparisons correction was applied. Second, individual series were short (21–181 systolic frames; median 29), limiting power and contributing to frequent "neither" phenotypes. All findings require independent replication. Third, MR jet area is load-dependent and not a standalone severity metric; it was used as a high-temporal-resolution surrogate where within-patient relative fluctuations remain informative for temporal coupling analysis. Fourth, patients were enrolled at three hospitals but selected for adequate image quality; multicentre replication with prospective enrolment is essential. Three observers performed measurements (one per patient); intraobserver reproducibility is reported in Supplementary Table S1. Fifth, a fixed lag of 3 (~100 ms) was used for individual models to maximise temporal coverage within the constraint of short series; sensitivity analyses at lags 1 and 2 yielded directionally consistent results. The pooled panel VAR assumes homogeneous lag structure within each subtype. Robustness across lags 2, 6, and 7 was confirmed. Sixth, longitudinal analysis was restricted to the anterolateral papillary muscle because consistent frame-level visualisation of the posteromedial papillary muscle was not achievable in all patients. Seventh, in the pooled analysis, systolic frames were concatenated across patients with patient fixed effects; lagged observations could theoretically cross patient boundaries, though such transitions represent a negligible proportion of observations and are unlikely to materially influence results. Eighth, the VAR/Granger framework captures only linear temporal dependencies; nonlinear interactions such as threshold effects or multiplicative coupling between determinants would require machine learning approaches and are explored in a companion study.

Conclusion

Beat-to-beat VAR/Granger modelling reveals subtype-specific temporal signatures of FMR, with LV volume dominating within-beat prediction and distinct temporal windows of PM predictability emerging across subtypes. These findings suggest papillary geometry primarily modulates the structural substrate rather than driving rapid variability. All findings are hypothesis-generating and require prospective validation in independent cohorts.

References

1. Asgar AW, Mack MJ, Stone GW. Secondary mitral regurgitation in heart failure: pathophysiology, prognosis, and therapeutic considerations. J Am Coll Cardiol. 2015;65(12):1231-48.
2. Dudzinski DM, Hung J. Echocardiographic assessment of ischemic mitral regurgitation. Cardiovasc Ultrasound. 2014;12:46.
3. Blendea ED, Lazar RD, Moldovan MP, Eotvos CA, Mihus ID, Munteanu MI, et al. Causality analysis of the determinants of atrial functional mitral regurgitation. Eur Heart J Digit Health. 2026;7(Suppl 1).
4. Zoghbi WA, Levine RA, Flachskampf F, Grayburn P, Gillam L, Leipsic J, et al. Atrial Functional Mitral Regurgitation: A JACC: Cardiovascular Imaging Expert Panel Viewpoint. JACC Cardiovasc Imaging. 2022;15(11):1870-82.
5. Huang AL, Dal-Bianco JP, Levine RA, Hung JW. Secondary Mitral Regurgitation: Cardiac Remodeling, Diagnosis, and Management. Struct Heart. 2023;7(3):100129.
6. Bartko PE, Heitzinger G, Spinka G, Pavo N, Prausmuller S, Kastl S, et al. Principal Morphomic and Functional Components of Secondary Mitral Regurgitation. JACC Cardiovasc Imaging. 2021;14(12):2288-300.
7. Yiu SF, Enriquez-Sarano M, Tribouilloy C, Seward JB, Tajik AJ. Determinants of the degree of functional mitral regurgitation in patients with systolic left ventricular dysfunction: A quantitative clinical study. Circulation. 2000;102(12):1400-6.
8. Stone GW, Lindenfeld J, Abraham WT, Kar S, Lim DS, Mishell JM, et al. Transcatheter Mitral-Valve Repair in Patients with Heart Failure. N Engl J Med. 2018;379(24):2307-18.
9. Obadia JF, Messika-Zeitoun D, Leurent G, Iung B, Bonnet G, Piriou N, et al. Percutaneous Repair or Medical Treatment for Secondary Mitral Regurgitation. N Engl J Med. 2018;379(24):2297-306.
10. Avram T, Apetrei C-A, Blendea E, Munteanu M, Mihus I-D, Moldovan M, et al. Abstract 4367285: Short-Term Determinants of Atrial and Ventricular Functional Mitral Regurgitation: Insights from Impulse Response Modeling. Circulation. 2025;152(Suppl_3):A4367285-A.

11. Naser JA, Kucuk HO, Ciobanu AO, Jouni H, Oguz D, Thaden JJ, et al. Atrial fibrillation is associated with large beat-to-beat variability in mitral and tricuspid annulus dimensions. Eur Heart J Cardiovasc Imaging. 2021.

12. Addetia K, Lang RM. Beat-to-beat variability occurs not only in atrial fibrillation: clinical value of dynamic assessment of the mitral and tricuspid annulus. Eur Heart J Cardiovasc Imaging. 2021.

13. Moraldo M, Cecaro F, Shun-Shin M, Pabari PA, Davies JE, Xu XY, et al. Evidence-based recommendations for PISA measurements in mitral regurgitation: systematic review, clinical and in-vitro study. Int J Cardiol. 2013;168(2):1220-8.

14. Olgun Kucuk H, Jouni H, Oguz D, Thaden JJ, Nkomo VT, Pislaru C, et al. Large, Unpredictable Beat-To-Beat Variability of Mitral Annulus Size in Atrial Fibrillation: Implications for Percutaneous Interventions. JACC Cardiovasc Interv. 2020;13(11):1387-9.

15. Granger CWJ. Investigating Causal Relations by Econometric Models and Cross-spectral Methods. Econometrica. 1969;37(3):15.

16. Handa BS, Li X, Aras KK, Qureshi NA, Mann I, Chowdhury RA, et al. Granger Causality-Based Analysis for Classification of Fibrillation Mechanisms and Localization of Rotational Drivers. Circ Arrhythm Electrophysiol. 2020;13(3):e008237.

17. Buccheri S, Sarno G, Frobert O, Gudnason T, Lagerqvist B, Lindholm D, et al. Assessing the Nationwide Impact of a Registry-Based Randomized Clinical Trial on Cardiovascular Practice. Circ Cardiovasc Interv. 2019;12(3):e007381.

18. Barker J, Sau A, Bajaj N, Jenkins A, Sharp A, Shi X, et al. Granger causality connectivity analysis of persistent atrial fibrillation dynamics reveals posterior wall mechanistic insights. Heart Rhythm O2. 2025;6(8):1097-105.

19. Kisanuki A, Otsuji Y, Kuroiwa R, Murayama T, Matsushita R, Shibata K, et al. Two-dimensional echocardiographic assessment of papillary muscle contractility in patients with prior myocardial infarction. J Am Coll Cardiol. 1993;21(4):932-8.

20. Magne J, Pibarot P, Dagenais F, Hachicha Z, Dumesnil JG, Senechal M. Preoperative posterior leaflet angle accurately predicts outcome after restrictive mitral valve annuloplasty for ischemic mitral regurgitation. Circulation. 2007;115(6):782-91.

21. Coats AJS, Anker SD, Baumbach A, Alfieri O, von Bardeleben RS, Bauersachs J, et al. The management of secondary mitral regurgitation in patients with heart failure: a joint position statement from the Heart Failure Association (HFA), European Association of Cardiovascular Imaging (EACVI), European Heart Rhythm Association (EHRA), and European Association of Percutaneous Cardiovascular Interventions (EAPCI) of the ESC. Eur Heart J. 2021;42(13):1254-69.

22. Upadhyay GA, Chatterjee NA, Kandala J, Friedman DJ, Park MY, Tabtabai SR, et al. Assessing mitral regurgitation in the prediction of clinical outcome after cardiac resynchronization therapy. Heart Rhythm. 2015;12(6):1201-8.

Ethics statement

This retrospective study was conducted in accordance with the Declaration of Helsinki. Institutional review board approval was obtained from the Ethics Committee of Iuliu Hațieganu University of Medicine and Pharmacy, Cluj-Napoca, Romania (approval number 216, 20 July 2022). Written informed consent was obtained from all participants prior to enrolment. Data from 41 consecutive patients with functional mitral regurgitation were retrospectively analysed.

Data availability

The de-identified patient-level dataset is archived on Zenodo (10.5281/zenodo.19396466) and available upon reasonable request to the corresponding author, subject to a data use agreement. The Stata analysis code is archived on Zenodo (10.5281/zenodo.19396431) and freely available at https://github.com/dblendea/FMR_causality.

Author contributions

All authors contributed to the conception and design of the study, interpretation of data, drafting and critical revision of the manuscript, and approved the final version for submission. D Blendea and CA Eotvos had primary responsibility for the final content.

Conflicts of interest

Teodora Avram — Speaker fees: Boehringer Ingelheim. Madalina P. Moldovan — Speaker fees: Boehringer Ingelheim. E. Kevin Heist — Consultant: Boston Scientific, Biotronik, Future Cardia. Dan Blendea — Speaker fees:

Boehringer Ingelheim, Pfizer, Berlin-Chemie, Merck, Abbott; Consultant: Voiant. All other authors declare no conflicts of interest.

Tables

Table 1. Baseline Characteristics by MR Severity — Mild vs Moderate–Severe

	AFMR (n=21)			**VFMR (n=20)**			**Overall (n=41)**		
Variable	**Mild (n=10)**	**Mod–Sev (n=11)**	**p**	**Mild (n=8)**	**Mod–Sev (n=12)**	**p**	**Mild (n=18)**	**Mod–Sev (n=23)**	**p**
Demographics									
Age (years)	81.8 (7.6)	79.6 (7.2)	0.511	63.5 (9.8)	69.0 (7.9)	0.182	73.7 (12.6)	74.1 (9.1)	0.902
Female sex	8 (80%)	8 (73%)	1.000	1 (12%)	2 (17%)	1.000	9 (50%)	10 (43%)	0.758
CAD	2 (20%)	0 (0%)	0.214	6 (75%)	8 (67%)	1.000	8 (44%)	8 (35%)	0.748
Hypertension	9 (90%)	10 (91%)	1.000	6 (75%)	9 (75%)	1.000	15 (83%)	19 (83%)	1.000
Diabetes	2 (20%)	2 (18%)	1.000	4 (50%)	3 (25%)	0.356	6 (33%)	5 (22%)	0.489
Obesity	8 (80%)	7 (64%)	0.635	6 (75%)	5 (42%)	0.197	14 (78%)	12 (52%)	0.114
AF history	8 (80%)	9 (82%)	1.000	2 (25%)	5 (42%)	0.642	10 (56%)	14 (61%)	0.760
NYHA class	2.5 (0.5)	2.2 (0.6)	0.215	2.2 (0.5)	2.8 (0.6)	0.068	2.4 (0.5)	2.5 (0.7)	0.638
Heart rate (bpm)	75.7 (11.4)	78.0 (24.9)	0.792	73.9 (14.8)	76.6 (19.6)	0.744	74.9 (12.6)	77.3 (21.8)	0.684
QRS duration (ms)	103.3 (22.6)	104.2 (32.2)	0.943	95.6 (15.2)	129.3 (39.6)	**0.035**	99.9 (19.5)	117.3 (37.7)	0.083
LBBB	2 (20%)	3 (27%)	1.000	0 (0%)	6 (50%)	**0.042**	2 (11%)	9 (39%)	0.075
MR Characteristics									
MR grade (1–4)	1.0 (0.0)	3.0 (0.8)	**<0.001**	1.0 (0.0)	2.6 (0.7)	**<0.001**	1.0 (0.0)	2.8 (0.7)	**<0.001**
TR grade	1.5 (0.7)	2.1 (0.5)	**0.043**	0.9 (0.6)	1.6 (0.8)	0.050	1.2 (0.7)	1.8 (0.7)	**0.012**
Pulmonary hypertension	5 (50%)	8 (73%)	0.387	1 (12%)	3 (25%)	0.762	6 (33%)	11 (48%)	0.426
Left Ventricular Parameters									
LVEDD (mm)	45.5 (2.2)	48.6 (7.4)	0.214	47.6 (3.4)	57.2 (8.4)	**0.007**	46.4 (2.9)	53.1 (8.9)	**0.004**
LVESD (mm)	31.4 (3.3)	31.5 (7.9)	0.984	37.1 (6.3)	47.6 (10.0)	**0.017**	33.9 (5.5)	39.9 (12.1)	0.062
LVEDV (ml)	86.6 (22.3)	101.7 (24.9)	0.160	157.9 (98.1)	189.1 (112.9)	0.532	118.3 (74.5)	147.3 (93.0)	0.287
Ejection fraction (%)	58.2 (7.6)	55.0 (4.6)	0.256	43.0 (7.3)	32.6 (12.3)	**0.045**	51.4 (10.6)	43.3 (14.7)	0.055
LV length early systole (cm)	6.2 (0.5)	5.8 (1.0)	0.360	7.6 (1.0)	8.2 (1.1)	0.211	6.8 (1.0)	7.1 (1.6)	0.542

LV length end systole (cm)	5.8 (0.6)	5.6 (0.9)	0.516	6.7 (1.0)	7.7 (1.2)	0.085	6.2 (0.9)	6.7 (1.5)	0.244
IVS thickness (mm)	12.0 (1.7)	11.5 (2.6)	0.579	12.5 (1.8)	10.3 (2.1)	**0.026**	12.2 (1.7)	10.9 (2.3)	**0.046**
PW thickness (mm)	11.6 (2.2)	11.3 (2.3)	0.743	11.2 (2.1)	9.8 (1.5)	0.093	11.4 (2.1)	10.5 (2.0)	0.161
Left Atrial Parameters									
LA diameter (mm)	50.0 (5.2)	54.9 (18.2)	0.421	40.3 (6.3)	39.9 (5.4)	0.882	45.7 (7.4)	47.1 (14.9)	0.720
LA volume (ml)	100.9 (40.6)	217.1 (321.6)	0.272	72.4 (24.3)	66.2 (31.1)	0.641	88.2 (36.4)	138.3 (231.1)	0.369
Mitral Valve Geometry									
MV annulus end-systole (cm)	2.5 (0.6)	2.9 (0.6)	0.078	2.9 (0.6)	3.0 (0.7)	0.790	2.7 (0.6)	3.0 (0.6)	0.117
MV annulus end-diastole (cm)	2.6 (0.6)	3.2 (0.6)	**0.025**	3.1 (0.6)	3.3 (0.6)	0.458	2.8 (0.7)	3.2 (0.6)	**0.023**
Tenting height early systole (cm)	1.0 (0.2)	1.0 (0.4)	0.751	1.0 (0.1)	1.2 (0.3)	**0.048**	1.0 (0.2)	1.1 (0.4)	0.122
Tenting height end-systole (cm)	0.8 (0.3)	0.8 (0.4)	0.710	0.8 (0.2)	1.0 (0.3)	0.181	0.8 (0.2)	0.9 (0.3)	0.213
Tenting area early systole (cm^2)	2.0 (0.7)	2.2 (1.2)	0.782	2.0 (0.9)	3.0 (1.6)	0.123	2.0 (0.8)	2.6 (1.5)	0.130
Tenting area end-systole (cm^2)	1.5 (0.8)	1.8 (1.0)	0.556	1.9 (0.8)	2.7 (1.6)	0.202	1.7 (0.8)	2.2 (1.4)	0.135
Papillary Muscle Length									
ALPM length 4-ch (cm)	2.8 (0.4)	2.5 (0.5)	0.119	2.8 (0.8)	3.0 (0.8)	0.652	2.8 (0.6)	2.7 (0.7)	0.777
PMPM length PS (cm)	3.6 (0.6)	3.7 (1.1)	0.830	4.1 (1.5)	3.7 (0.7)	0.388	3.8 (1.1)	3.7 (0.9)	0.637

Data presented as mean (SD) for continuous variables and n (%) for categorical variables. p values from independent samples t-test (continuous) or Fisher's exact test (categorical). Bold p values indicate p<0.05. Mild = MR grade 1; Moderate–Severe = MR grade ≥2. AFMR = atrial functional mitral regurgitation; VFMR = ventricular functional mitral regurgitation; CAD = coronary artery disease; AF = atrial fibrillation; LBBB = left bundle branch block; LVEDD = LV end-diastolic diameter; LVESD = LV end-systolic diameter; LVEDV = LV end-diastolic volume; EF = ejection fraction; LA = left atrium; MV = mitral valve; ALPM = anterolateral papillary muscle; PMPM = posteromedial papillary muscle.

Table 2. Individual Patient VAR Granger Causality Results

Pt	**N**	**LA volume → MR area**			**LV volume → MR area**			**ALPM length → MR area**			**Phenotype**
		p	**IRF**	**FEVD%**	**p**	**IRF**	**FEVD%**	**p**	**IRF**	**FEVD%**	
AFMR (n=21; 14 stable at lag 3, 4 excluded <20 frames, 3 unstable)											
1	28	0.551	↑	5.6	**0.011**	↑	6.4	**<.001**	↑	42.4	**LV+PM** †
2	29	---	↑	13.8	---	↓	0.2	---	↓	10.0	**Neither** †
3	33	**<.001**	↓	33.1	**<.001**	↑	7.7	**<.001**	↓	50.1	**LV+PM**
4	29	**0.006**	↑	18.7	**0.030**	↑	12.2	---	---	---	**LA+LV**

Pt	N	LA volume → MR area			LV volume → MR area			ALPM length → MR area			Phenotype
		p	IRF	FEVD%	p	IRF	FEVD%	p	IRF	FEVD%	
5	29	0.555	↓	1.8	0.139	↑	17.5	---	---	---	**Neither**
6	29	**0.024**	↑	33.1	0.412	↓	0.8	---	---	---	**LA-dominant**
8	68	0.058	↓	2.6	**0.033**	↑	8.0	---	---	---	**LV-dominant**
11	31	0.052	↓	1.8	0.672	↑	10.4	**0.008**	↑	16.5	**PM-dominant**
12	29	**0.015**	↓	16.7	0.702	↑	13.4	0.168	↓	13.0	**LA-dominant**
13	29	**0.022**	↑	25.7	0.178	↑	6.0	0.679	↓	2.0	**LA-dominant**
14	29	**0.010**	↓	17.6	0.314	↓	18.3	0.239	↑	6.6	**LA-dominant**
15	29	0.072	↑	5.2	0.247	↑	7.7	0.496	↓	6.2	**Neither**
16	29	0.387	↓	4.1	0.139	↑	10.6	0.091	↓	12.0	**Neither**
17	29	0.465	↑	29.3	0.727	↓	1.6	0.619	↓	0.9	**Neither**
18	29	**0.020**	↓	16.9	**0.025**	↑	12.8	0.937	↑	5.5	**LA+LV**
19	29	**0.002**	↑	22.2	0.092	↓	9.6	**0.020**	↑	11.7	**LA+PM**
20	51	0.118	↑	6.6	**<.001**	↑	18.3	**0.007**	↑	13.2	**LV+PM** *†*
VFMR (n=20; 11 stable at lag 3, 3 excluded <20 frames, 6 unstable)											
22	57	**<.001**	↓	34.5	**<.001**	↑	13.1	0.061	↑	14.6	**LA+LV**
23	25	---	↓	11.7	---	↑	0.3	---	↓	0.8	**Neither** *†*
24	32	**<.001**	↑	25.1	**0.029**	↓	20.2	0.684	↑	2.2	**LA+LV**
25	30	0.123	↑	5.9	**<.001**	↓	42.1	**<.001**	↓	2.1	**LV+PM** *†*
26	39	**<.001**	↑	39.4	**0.007**	↑	12.3	**0.012**	↓	8.1	**LV+PM**
27	34	**0.031**	↓	20.4	**0.037**	↑	7.0	0.158	↓	18.9	**LA+LV**
28	22	**<.001**	---	---	**<.001**	---	---	**<.001**	---	---	**LV+PM** *†*
29	181	0.059	↑	2.6	**<.001**	↑	14.9	**0.001**	↑	10.2	**LV+PM**
30	30	**<.001**	↓	35.2	0.058	↑	6.6	0.515	↓	1.4	**LA-dominant**
31	32	**0.031**	↓	8.1	**0.027**	↑	8.8	0.138	↑	14.1	**LA+LV**
32	30	0.085	↓	4.3	**0.019**	↑	6.6	**0.032**	↑	33.2	**LV+PM**
34	32	**0.006**	↓	40.4	0.766	↑	4.2	0.428	↓	7.6	**LA-dominant**
35	30	0.669	↑	3.3	0.071	↓	12.5	0.427	↑	12.4	**Neither** *†*
36	25	0.170	↓	13.1	**<.001**	↓	23.4	**0.002**	↑	13.0	**LV+PM**
39	21	---	↑	14.8	---	↑	1.8	---	↓	0.6	**Neither** *†*
40	32	0.359	↑	9.7	0.441	↓	6.8	0.871	↑	0.1	**Neither** *†*
41	29	0.152	↑	17.8	0.715	↓	3.8	0.534	↑	2.4	**Neither**

*AFMR = atrial functional MR; VFMR = ventricular functional MR; LA = left atrium; LV = left ventricle; ALPM = anterolateral papillary muscle; p = Granger causality Wald test p-value; IRF = orthogonalised impulse response function sign at step 1 (↑ positive, ↓ negative); FEVD% = forecast error variance decomposition at horizon 5 (percentage of MR variance explained). All results from VAR(3) models (~100 ms at 30 fps). Full model: 4-variable (MR, LV vol, LA vol, ALPM); Reduced (—): 3-variable (MR, LV vol, LA vol; ALPM not visible). Bold = p<0.05. † Unstable VAR (eigenvalue ≥1); results interpreted with caution. * Patient 40: structural post-MI ALPM dysfunction; no dynamic Granger causality (see Results text). Median systolic frames per analysed patient: 29 (range 21–181).*

Table 3. Pooled VAR Granger Causality — Beat-to-Beat Predictors of MR Area

		AFMR (17 pts)			**VFMR (20 pts)**			**Overall (37 pts)**		
Phase	**Lag**	**p**	**IRF**	**FEVD**	**p**	**IRF**	**FEVD**	**p**	**IRF**	**FEVD**
LA volume → MR area										
Systolic	2	0.509		0.0	**0.018**	+	0.7	**<0.001**	+	0.8
Systolic	6	**0.033**	-	0.5	**0.004**	+	1.1	**<0.001**	+	1.1
Systolic	7	**0.043**	-	0.5	**0.011**	+	1.2	**<0.001**	+	1.1
LV volume → MR area										
Systolic	2	**0.011**	+	2.1	**0.006**	+	1.9	**<0.001**	+	2.2
Systolic	6	**0.012**	+	2.3	0.328		1.0	**0.009**	+	1.8
Systolic	7	**0.047**	+	1.5	0.313		0.9	**0.044**	+	1.3
ALPM length → MR area										
Systolic	2	0.457	−	0.5	0.831		0.2	0.977		0.01
Systolic	6	0.295		1.0	0.819		0.02	0.884		0.1
Systolic	7	0.210		1.2	0.707		0.03	0.243		0.1
Annulus diameter → MR area										
Systolic	2	0.966	−	0.0	0.238	−	0.6	0.116	−	0.5
Systolic	6	**0.033**	−	0.2	**0.017**	−	0.03	0.436		0.3

Systolic	7	**0.027**	−	0.3	**0.011**	+	0.06	0.349		0.2
ALL predictors (joint Granger test)										
Systolic	2	0.252	—	—	**0.029**	—	—	**<0.001**	—	—
ALPM length → MR area (full-cycle model ‡)										
Full cycle	1	0.314		0.3	**0.001**	+	1.3	—		
Full cycle	2	0.544		0.4	**0.005**	+	1.3	—		
Full cycle	4	0.502		0.5	**0.030**	+	1.4	—		
Full cycle	7	0.411		0.9	**0.040**	+	1.5	—		
MR area → ALPM length (reverse Granger, full-cycle model ‡)										
Full cycle	1	**0.016**		1.4	0.289		2.2	—		
Full cycle	2	**<0.001**		3.8	0.359		2.0	—		
Full cycle	4	**<0.001**		6.4	0.183		3.0	—		
Full cycle	7	**<0.001**		6.7	0.621		2.5	—		

Pooled VAR with patient fixed effects; 5 endogenous variables (MR area, LV volume, LA volume, systolic ALPM length, annulus diameter). p = Granger causality Wald χ^2 test; bold = p<0.05. IRF = impulse response sign at step 1 (shown only for significant predictors). FEVD = forecast error variance decomposition at horizon 5 (% of MR area variance). All models stable. † 4 AFMR patients excluded (absent ALPM); ‡ Full-cycle rows: 4-variable model (MR area, LV volume, LA volume, ALPM length); z-scores standardised across full cardiac cycle; FEVD at horizon 10.

Figures

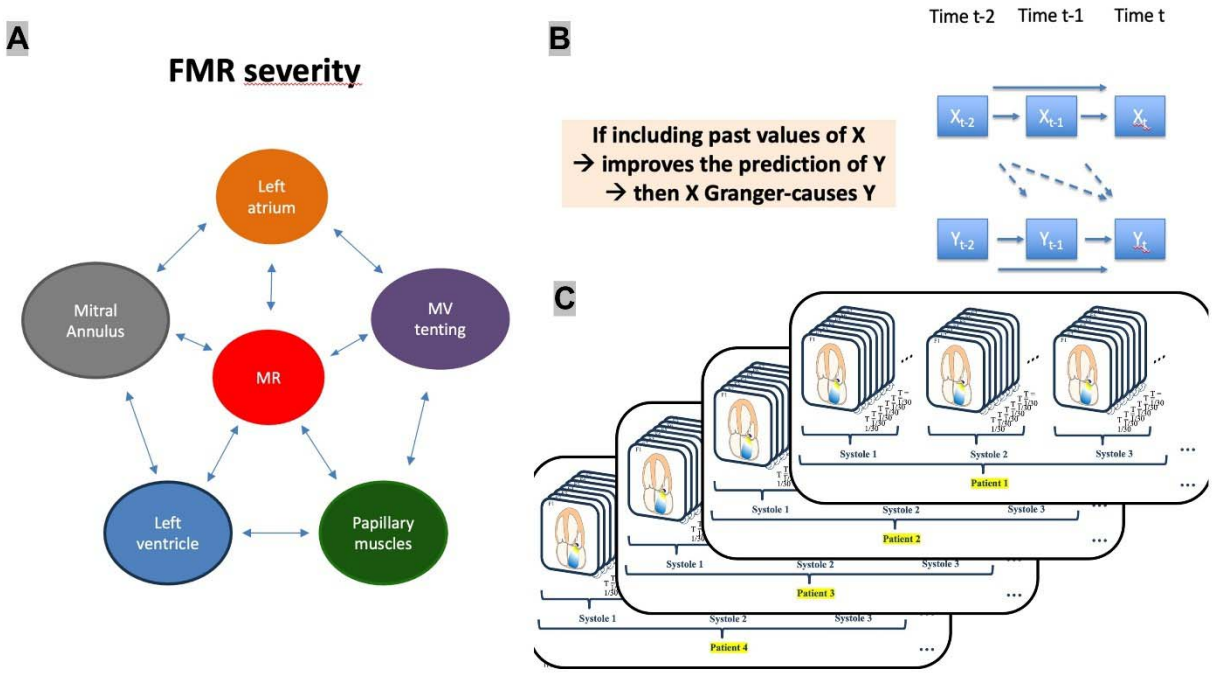

Figure 1. Panel A: Conceptual framework of beat-to-beat Granger-predictive modelling in FMR. The determinant network shows how MR jet area variability is influenced by LV volume, LA volume, annulus diameter, and ALPM length within each cardiac cycle. Bidirectional arrows indicate tested Granger-predictive pathways; **Panel B**: Temporal logic of Granger causality testing. Past values of variable X at lags t−2 and t−1 are tested as predictors of variable Y at time t, conditional on Y's own history. If including past values of X improves prediction of Y beyond Y's autoregressive component, X is said to Granger-cause Y. In this study, X represents each structural determinant (LV volume, LA volume, ALPM length, annulus diameter) and Y represents MR area. **Panel C**: Schematic of frame-by-frame echocardiographic acquisition showing systolic frame labelling across consecutive cardiac cycles. ALPM = anterolateral papillary muscle; FMR = functional MR; LA = left atrium; LV = left ventricle; MR = mitral regurgitation.

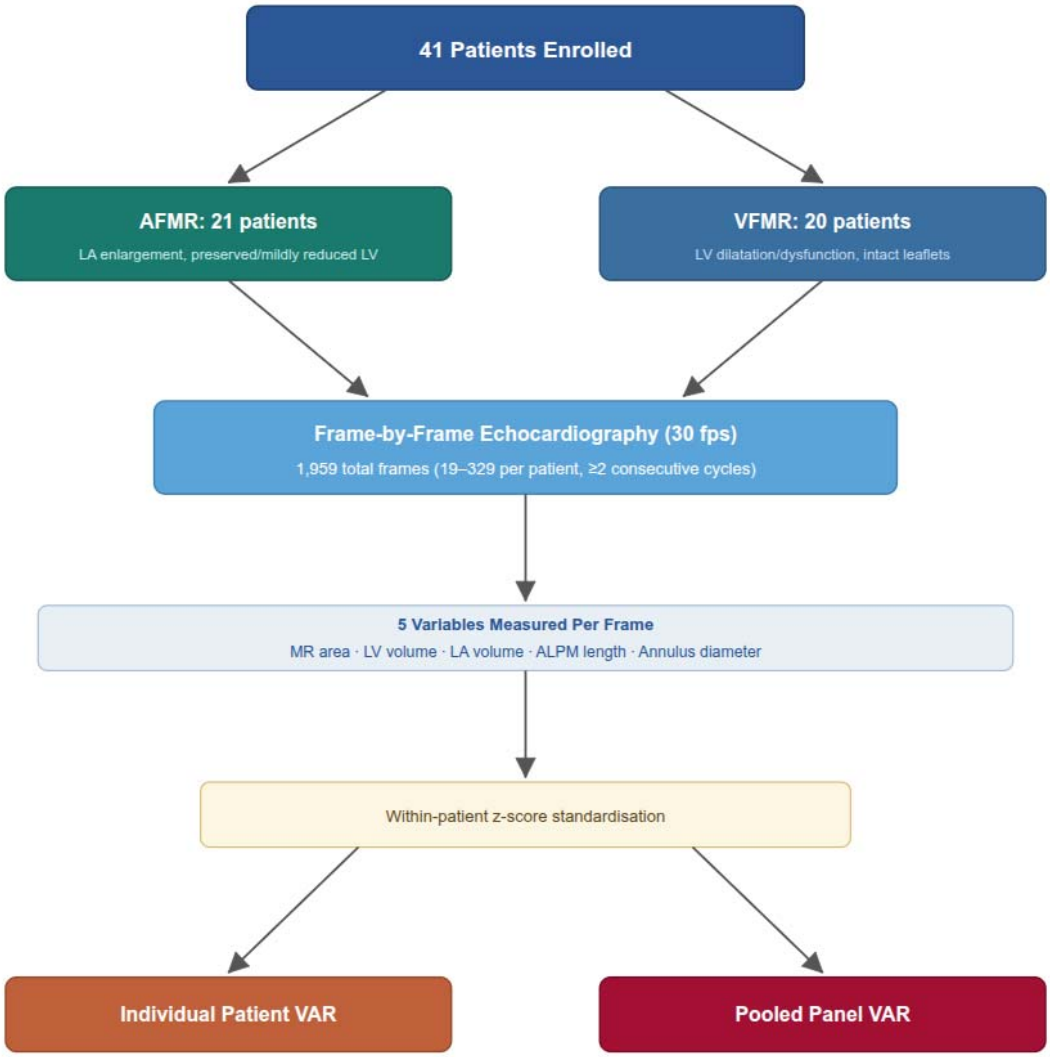

Figure 2. Study flow, phenotype classification, and VAR analysis framework.

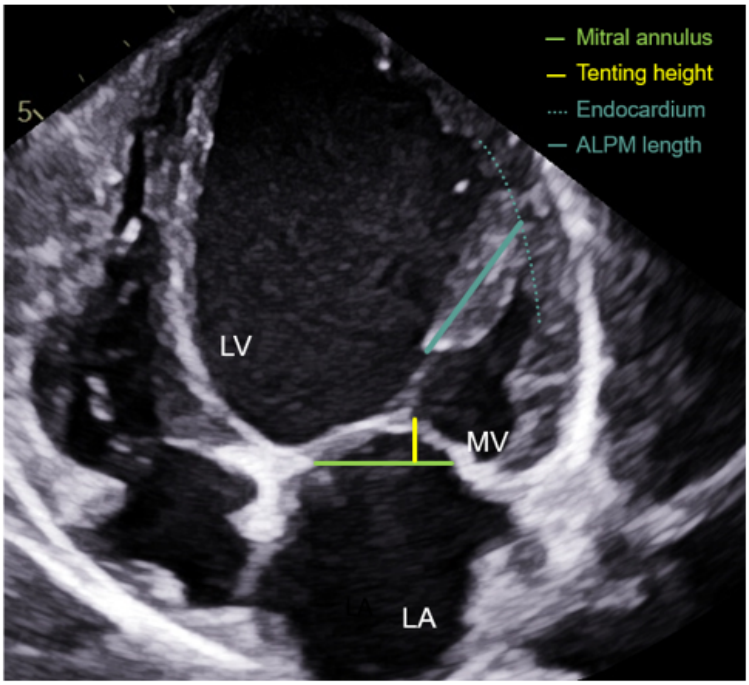

Figure 3. Four-chamber apical view illustrating key structural measurements of the mitral valve apparatus. The mitral annulus (green line) and tenting height (yellow line) are shown, along with the endocardial contour (dotted line). Anterolateral papillary muscle (ALPM) length (blue line) was measured as the distance from the LV apex to its mid-basal insertion along the endocardial border.

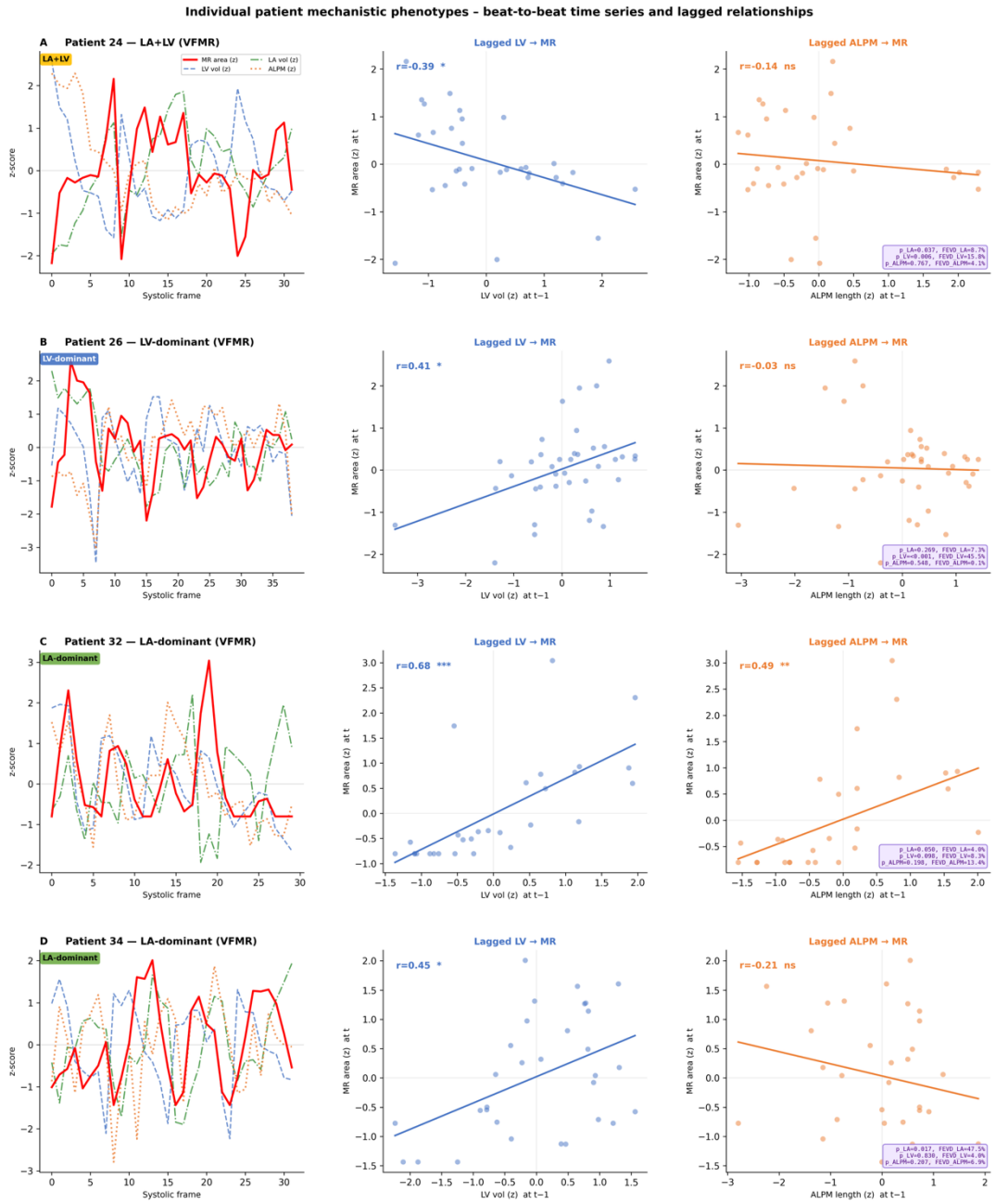

Figure 4. Individual-patient Granger-predictive phenotypes. Each patient is classified by the dominant frame-level Granger predictor of MR jet area (LV volume, LA volume, or papillary muscle length). Classification based on Wald FEVD at horizon 5. Phenotype labels correspond to Table 2. AFMR = atrial functional MR; VFMR = ventricular functional MR

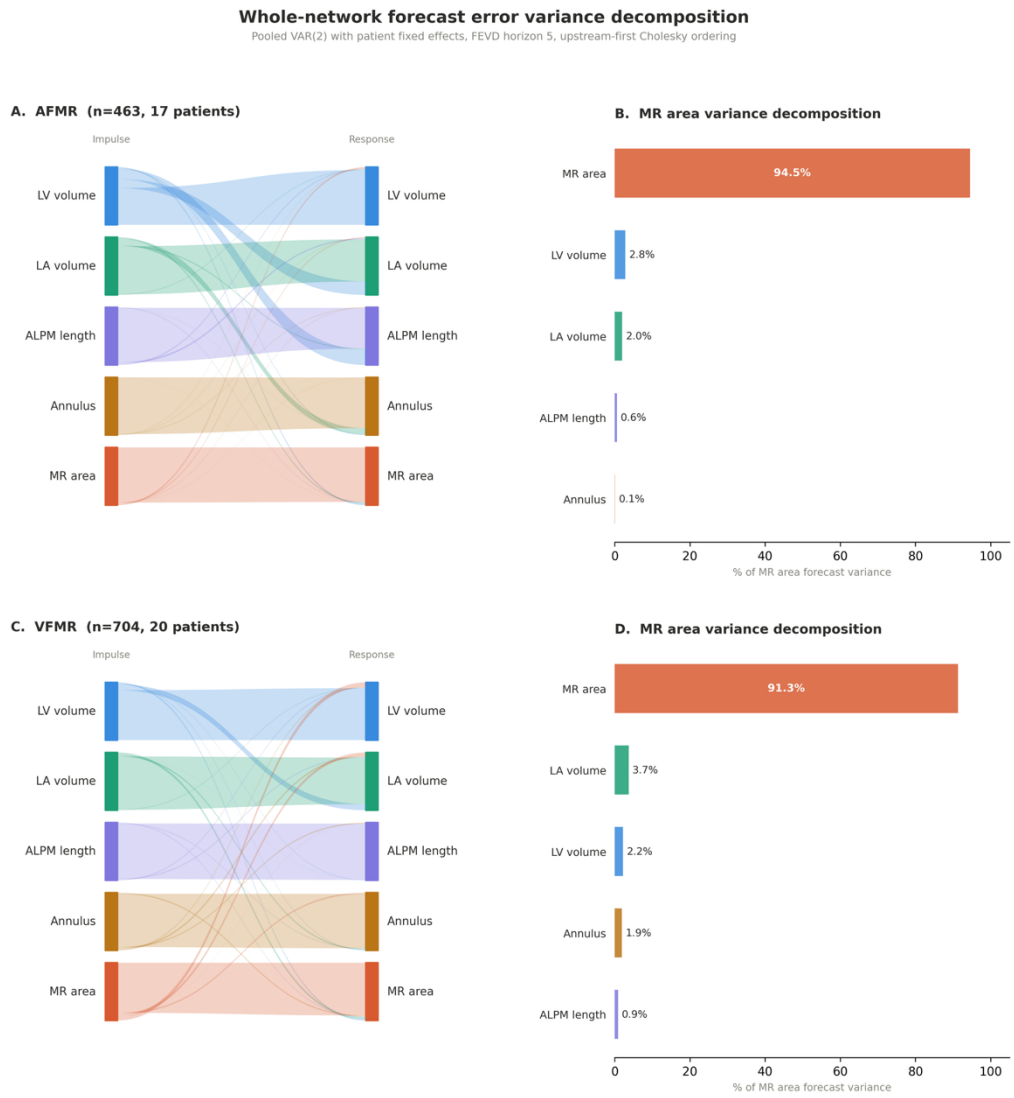

Figure 5. Whole-network forecast error variance decomposition in AFMR (A) and VFMR (B). Pooled VAR(2) with patient fixed effects, FEVD at horizon 5, upstream-first Cholesky ordering. Ribbon width represents the percentage of forecast variance in the response variable explained by the impulse variable. Bar charts show the MR area variance breakdown for each subtype.